A Physiologically Based Pharmacokinetic Model to Predict Pegylated Liposomal Doxorubicin Disposition in Rats and Human

Maiara Camotti Montanha (m.camotti-montanha@liverpool.ac.uk)
University of Liverpool https://orcid.org/0000-0002-2078-360X
Alice Howarth
University of Liverpool
Doaa Ahmed Mohamed
University of Liverpool
Estelle Loier
University of Liverpool
Lauren Main
University of Liverpool
Matthias Rösslein
Swiss Federal Laboratories for Materials Science and Technology Thun: EMPA Thun Standort
Christiaan Delmaar
RIVM: Rijksinstituut voor Volksgezondheid en Milieu
Adriele Prina-Mello
Trinity College Dublin: The University of Dublin Trinity College
Marco Siccardi
University of Liverpool

Research Article

Keywords: Biodistribution, Doxil, in silico modelling, Nanoparticles, Physiologically Based Pharmacokinetic (PBPK).

Posted Date: March 11th, 2022

DOI: https://doi.org/10.21203/rs.3.rs-1417093/v1

Abstract

The use of nanoparticles (NPs) can support an enhancement of drug distribution, resulting in increased drug penetration into key tissues. Experimental in vitro data can be integrated into computational approaches to simulate NP absorption, distribution, metabolism, and elimination (ADME) processes and provide quantitative pharmacokinetic predictions. The aim of this study is to develop a novel mechanistic and physiologically based pharmacokinetic (m-PBPK) model to predict the biodistribution of NPs focusing on Doxil.

The main processes underpinning NPs ADME were represented considering molecular and cellular mechanisms such as stability in biological fluids, passive permeability, and uptake activity by macrophages. A whole-body m-PBPK rat and human models were designed in Simbiology v. 9.6.0 (MATLAB R2019a).

The m-PBPK models was successfully qualified across doxorubicin and Doxil® in both rat and human since all PK parameters AUC_{0-inf}, C_{max}, $t_{1/2}$, Vd and Cl were within 2-fold, with an AUC_{0-inf} absolute average-fold error (AAFE) value of 1.23 and 1.16, and 1.76 and 1.05 for Doxorubicin and Doxil® in rat and human, respectively. The time to maximum concentration in tissues for doxorubicin in both rat and human models was before 30 minutes of administration, while for Doxil® the tmax was after 24 hours of administration. The organs that accumulate most NP are spleen, liver, and lungs, in both models.

The m-PBPK represents a predictive platform for the integration of in vitro and formulation parameters in a physiological context to quantitatively predict the NP biodistribution.

Introduction

Nanomedicine strategies have emerged as an advanced approach to enhance drug delivery and targeting across multiple disease areas over the past 20 years. New formulation opportunities can overcome the limitations associated with traditional drug therapies supporting the advancement of therapeutic (enhancement of efficacy, protection of drugs from degradation or targeting) and diagnostic functions [1].

Doxil® was the first liposome approved by the Food and Drug Administration (FDA) in 1995 for the treatment of Kaposi's sarcoma followed by European approval in 1997 [1]. This liposome contains a DNA intercalating agent: doxorubicin, which is an anthracycline isolated from the bacterium *Streptomyces peucetius* [2]. These liposomal anthracyclines are more effective and have reduced side effects including cardiotoxicity, nausea and alopecia compared to the free drug.

Doxil® are stealth liposomes, made with PolyEthylene Glycol (PEG) coating, to inhibit protein adhesion (opsonization) and to delay the recognition by the Mononuclear Phagocyte System (MPS) following intravenous (IV) administration. The PEG coating extends circulation time to 3–4 days in humans [3]. Moreover, due to their size of approximately 100 nm [1], liposomes are designed to target solid tumours via the Enhanced Permeability and Retention (EPR) effect also called "passive targeting" [4]. This effect

has been well documented in rodents and contributes to the extravasation of Doxil® via convection through defenestrated blood vessels surrounding the tumour.

Once Doxil® has reached the Extra Cellular Matrix (ECM), its internalisation relies on effective cellular uptake via various endocytic pathways. More importantly, once Doxil® has reached the targeting tissue, it is retained from the general circulation due to the limited lymphatic drainage system of tumour tissues [5]. Drug release from the liposomal formulation is an important parameter that must be considered, not only within tumour cells but also within the systemic circulation. Insufficient drug release at the tumour site can lead to a lack of efficacy [6], whereas significant drug release in the bloodstream could increase systemic side effects while preventing the compound from reaching the target tissue.

Among nanomedicines, liposomes are the most used in chemotherapy and despite their advantages, they are still associated with side effects [7]. Doxil® has two major side effects. The first is severe dermatitis called Palmar Plantar Erythrodysthesia (PPE) or “foot and hand syndrome” and the second is characterised by shortness of breath. Therefore, dose is limited by these two effects and this more globally impacts the pharmacokinetic profile [6].

Physiologically based pharmacokinetic (PBPK) modelling is based on the integration of the mathematical description of anatomical, physiological, and molecular processes underpinning pharmacokinetics with *in vitro* data, to describe ADME [8]. While the pre-clinical approach evaluates various physicochemical, biophysical, and physiological factors in isolation, PBPK modelling can be applied systemically where multiple factors can be investigated at establishing the importance of the key variables such as NP cellular interactions, effects of hemodynamic on intravascular NP transport, and the relevance of NP properties and tumour microenvironment for the delivery of NPs to the tumour [9].

Moreover, with the increase of requirements from regulatory agencies to reduce the use of animal studies (the 3Rs), the development of alternative methods such as PBPK modelling to assess the biodistribution of NP is a valuable tool. The aim of this study is to develop a novel m-PBPK model considering both rat and human physiology for the prediction of NBM biodistribution with a special focus on Doxil®.

Methods

Rat PBPK model structure

A whole-body mechanistic physiologically based pharmacokinetic (m-PBPK) rat model was designed in Simbiology v. 9.6.0 (MATLAB R2019a) and broken down in 16 compartments: blood, liver, spleen, kidneys, lungs, heart, brain, adipose tissue, bones, intestines, muscle, pancreas, skin, stomach, lymph central and remaining anatomical body features. The whole m-PBPK was also arranged in 2 blocks, the first one representing vascular and interstitial spaces for the nanoparticle, while for the released drug (doxorubicin) each organ was represented by the second block (Fig. 1). The physiological parameters organ volume and blood flow were described as previously by Peters [10], and the fraction of vascular

and interstitial space of each organ were described as by Shah and Betts [11]. The weight of organs was implemented as reported by the US Environmental Protection Agency [15].

Human PBPK model structure

A comparable 16 compartment structure model described for rats was used in the adult model. Physiological characteristics such as age, weight, and body mass index (BMI) were implemented as reported by the Centers for Disease Control and Prevention [13]. Organ and tissue volumes were calculated through weight anthropometric equations as described by Bosgra et al. [14]. Organ and tissue blood flows were calculated as a percentage of the cardiac output described by the US Environmental Protection Agency [15]. The fraction of vascular and interstitial space of each organ were calculated according to Gill et al. [12].

Distribution

The biodistribution of NP and released drug are represented differently [16] (Fig. 1). For the NP biodistribution two main processes were involved: (1) permeability of the NP across vascular wall into the interstitial compartment, (2) macrophage uptake of the NP into the tissue. The permeation of the NPs from the vascular space to the interstitial space considered both perfusion- and diffusion-limited approaches. Organs were grouped according to their capillary type as described before [17, 18] and adapted to the model here presented and summarised in the Table 1.

The distribution of the released drug (doxorubicin) into organs and tissues was simulated using previously published equations, and tissue-to-plasma ratios (TP) were calculated according to Poulin and Theil's equations [19]. The tissue composition (fractional tissue volume content of phospholipid, neutral lipid, and water) of each organ for rats and human was used as described previously by Peters [10].

Table 1
Transcapillary permeability according to specific organs.

Blood capillary type	Organs	Transcapillary permeability
CT1 (non-sinusoidal non-fenestrated)	Heart, lungs, brain, bones, muscle, adipose, skin, stomach, remaining	0.0015
CT2 (non-sinusoidal fenestrated)	Intestines, pancreas, kidneys	0.012
CT3 (sinusoidal with pores larger)	Liver, spleen	0.024
CT4 (myeloid bone marrow sinusoidal)	Bone marrow	0.216
Adapted from Sarin et al. [17] and Bachler et al. [18].		

Doxil® availability for each tissue vascular compartment was represented through the arterial organ blood flow (Q_{organ}, mL/h and L/h for rat and human models, respectively) and the venous organ blood flow (organ blood flow reduced by organ lymphatic flow, Q_{organ}- $Q_{L,organ}$). The $Q_{L,organ}$ was collected into a single compartment (lymph central) and was considered 500 times lower than the corresponding Q_{organ} as previously described[11]. It was assumed that lymph node fluid reabsorption is negligible, then the total lymph flow returning to the vein compartment was the sum of all organs lymph flow to keep a fluid balance [12]. Lymphatic flow from the spleen and bones tissues were considered negligible. A lymphatic reflection coefficient (σ_{lymph}) of 0.2 was set up according to previously published literature [11].

The amount of NP transported across the vascular wall was calculated considering the organ blood flow (Q_{organ}) normalized to the total body blood volume (V_{blood}) multiplied by the organ transcapillary permeability (CT):

$$NP_{influx}\ (mg/h) = \frac{Qorgan}{Vblood} \times CT \times NP \times fup, \quad Eq.\ 1$$

$$NP_{efflux}\ (mg/h) = \frac{Qorgan}{Vblood} \times CT \times NP \times fut, \quad Eq.\ 2$$

where NP is expressed as the mass of nanoparticles in the vascular or in the interstitial space in milligrams, and f_{up} and f_{ut} corresponds to the fraction unbound of the NP in the vascular space and in the tissue. It was assumed that there is no intracellular uptake of Doxil® or insignificant, once it is present mainly on vascular space, surrounding the blood vessels, and infiltrated into the extracellular space [20].

Macrophage uptake

Macrophage uptake of the NP from vascular to the interstitial space was calculated considering the *in vitro* macrophage uptake using primary cells, as previously published by some of the authors [21]. Subsequently, it was scaled up to macrophage clearance in the liver, spleen, and lungs as described in the Eqs. 3 and 4:

$$Cl_{int,MPS,organ} = Cl_{int,\,MPS} \times N_{macrophages} \times W_{organ}, \quad Eq.\ 3$$

$$Cl_{MPS,organ} = \frac{(Clint,\,macrophage,\,organ \times Qorgan)}{(Clint,\,macrophage,\,organ + Qorgan)}, \quad Eq.\ 4$$

where $Cl_{int,MPS}$, $N_{macrophages}$ and W_{organ} represent the *in vitro* macrophage intrinsic clearance (mL/min/cell), the number of macrophages per gram of organ and the weight of the organ in grams (liver, spleen, and lungs). The units of $Cl_{int,MPS,organ}$ and $Cl_{MPS,organ}$ were mL/h and L/h for rat and human models, respectively.

Metabolism and elimination

It was assumed in the model that the NP is phagocytosed by macrophages, dissolved, and doxorubicin released according to a macrophage release constant rate ($MPS_{release}$, h^{-1}). Doxorubicin is subsequently

metabolized and eliminated by apparent systemic clearance. A release rate constant (k_{deg}, h^{-1}) based on previous publication [22] was applied to consider the release of doxorubicin from the liposome in all compartments as shown in Fig. 1.

Model parametrization

All the NP and drug-specific parameters for the model are described in Table 2. Since the *in vitro* parameters $MPS_{release}$ and $Cl_{int,MPS}$ used as input in the model were not specific to Doxil®, initially they were adjusted in the rat model to match tissue accumulation values observed *in vivo*. After validation, these values were used in the human model to predict NP accumulation in different organs, since detailed human tissue distribution data is missing. The $N_{macrophages}$ per gram of tissue in rats was assumed the same as in mice. The values used in the model were: 8.6×10^5 for human liver, 1×10^7 for rat liver, 2×10^6 for human spleen, 4.5×10^6 for rat spleen, 1.1×10^6 for human lungs, and 3×10^7 for rat lungs [21]. The blood to plasma ratio (R) of Doxil® was considered 0.55 (Table 2) for rat and human (haematocrit in rats slightly higher than in humans) [20], since Doxil® does not bind to erythrocytes and is presented totally in the plasma. It was considered that a reduced or irrelevant amount of protein is adsorbed to its surface (f_{up} = 1), because it is a pegylated liposomal NP [20].

Table 2
Input parameters for the Doxil® and doxorubicin models in rat and human.

Parameter		Doxil®	Doxorubicin
Physicochemical			
Molecular weight (g/mol)		-	578 [23]
Log $P_{o:w}$		-	1.27 [23]
p*Ka*		-	9.53 (strongest acidic) 8.94 (strongest basic) [23]
f_{up}		1	0.02 [23]
R		0.55 *	2.4 [24]
PSA (Å^2)		-	206 [23]
HBD		-	6 [23]
Distribution			
V_{ss} correction factor	Rat	-	20
	Human	-	5
k_{deg} (h^{-1})		0.025 [22]	-
$MPS_{release}$ (h^{-1})		9 x 10^{-4} [21] 9 x 10^{-3} *	-
$Cl_{int,MPS}$ (mL/h/cell)		2.16 x 10^{-7} [21] 2.16 x 10^{-8} *	-
Elimination			
Cl_{syst}	Rat (mL/h)	-	321 ± 43.8 [24]
	Human (L/h)	-	25.3 (13.3–35.2) [25]

Log $P_{o:w}$ partition coefficient between octanol and water, p*K*a acid dissociation constant, *fup* fraction of drug unbound in plasma, R blood to plasma drug ratio, PSA polar surface area, HBD number of hydrogen bond donors, V_{ss} volume of distribution at steady-state, k_{deg} release constant rate, MPS release macrophage release constant rate, Cl_{int} macrophage intrinsic clearance in primary macrophage cells, Cl_{syst} apparent systemic clearance, - not applicable, *adjusted in the model considering haematocrit of 0.45.

Model qualification

The m-PBPK model was qualified using the administration of 6 mg/kg and 50 mg/m^2 of doxorubicin intravenously (IV) *in bolus* to rats and humans, respectively [26, 27]. The model was assumed to be qualified if the AAFE was below 2 when compared the predicted pharmacokinetic (PK) parameters AUC_{0-inf}, $t_{1/2}$, Vd and Cl to the observed data. The model was initially qualified with the IV administration of the released drug alone was to characterize the elimination phase (Cl_{syst}) to be subsequently applied to the NP model. The administration of 1 mg/kg of Doxil® IV *in bolus* to rats was simulated (Fig. 2) and the NP model was qualified against observed data [28, 29] in rats to adjust the parameters $MPS_{release}$ and $C_{lint,MPS}$ [21]. Finally, the same parameters used in the rat model were applied to the human NP m-PBPK model and the administration of 50 mg/m^2 of Doxil® IV (time of infusion 30 minutes) to humans was simulated (Fig. 3) and PK parameters were compared to the observed data [27].

Prediction of tissue distribution in rats and humans

Predictions of tissue accumulation in both rat and human models were simulated with administrations of 1 mg/kg and 50 mg/m^2 of Doxil® IV, respectively. The total concentration in tissue after 24 hours was calculated based on encapsulated + unencapsulated doxorubicin concentration. A sensitivity analysis of the rat model was performed considering the changes of Doxil® maximum concentration at 24 h in the liver, spleen, and lungs to a range variation of ± 10 and ± 5 times the initial value parameters: k_{deg}, $MPS_{release}$, $Cl_{int,MPS}$.

Results

Model qualification

The average weights in the rat model were 325.00 ± 14.65 g and 240.00 ± 5.90 g, while the average body-surface areas (BSA) in the human model were 1.85 ± 0.09 m^2 and 1.90 ± 0.10 m^2 (both to reflect observed data), when simulated the administration of doxorubicin and Doxil®, respectively. The m-PBPK models was successfully qualified across doxorubicin and Doxil® in both rat and human since all PK parameters AUC_{0-inf}, $C_{max,}$ $t_{1/2}$, Vd and Cl were within 2-fold (Table 3), with an AUC_{0-inf} AAFE value of 1.23 and 1.16, and 1.76 and 1.05 for Doxorubicin and Doxil® in rat and human, respectively (Table 3). The predicted doxorubicin unencapsulated concentration after administration of Doxil® (24 h after administration) was 0.1% or less of the total doxorubicin (0.035% in rats, 0.1% in human). Doxil® is characterised by a lower Cl, and an increased $t_{1/2}$ compared to doxorubicin (Table 3).

Table 3
PK parameters and model qualification of doxorubicin and Doxil® in both rat and human models.

	Rats					
Parameters	Doxorubicin (6 mg/kg)			Doxil® (1 mg/kg)		
	Observed [26]	Simulated	AAFE	Observed [28]	Simulated	AAFE
AUC (µg/mL.h)	1.95	2.40 (28.6)	1.23	605.3	700.3 (4.8)	1.16
$t_{1/2}$ (h)	3	2.33 (22.9)	1.29	27	30.8 (1.2)	1.14
Vd (mL)	3870	2740 (25.6)	1.41	16.5	15.2 (12.4)	1.08
Cl (mL/h)	863	813 (55.1)	1.06	0.4	0.3 (13)	1.17
	Humans					
Parameters	Doxorubicin (50 mg/m^2)			Doxil® (50 mg/m^2)		
	Observed [27]	Simulated	AAFE	Observed [27]	Simulated	AAFE
AUC (mg/L.h)	3.5	2 (29.7)	1.76	902	947 (8.0)	1.05
C_{max} (mg/L)	5.9	4 (6.7)	1.46	21.2	21.4 (9.1)	1.01
$t_{1/2}$ (h)	10.4	7.4 (23.3)	1.40	45.9	31.5 (2.8)	146
Vd (L)	365	459 (37.1)	1.26	5.9	0.09 (8.4)	1.0
Cl (L/h)	25.3	42.8 (8.9)	1.69	0.09	4.1 (5.6)	1.44

Data are presented as the mean (coefficient of variation, %). AUC_{0-inf}, area under the plasma concentration-time curve over a dosing interval. Abbreviations: C_{max} = maximum plasma concentration; $t_{1/2}$ = half-life time; Vd = volume of distribution and CL = clearance.

The sensitivity analysis considering tissue concentration at 24 h after the NP administration showed that increasing the degradation rate constant of Doxil® lead to an increase in unencapsulated drug availability for metabolism and excretion, and a decrease in the tissue C_{max}. The same behaviour was identified when increasing the $MPS_{release}$, since more unencapsulated drug is released and eliminated. The opposite is observed when an increment on $Cl_{int,MPS}$ is simulated, since more NP is uptake by the macrophage and higher C_{max} for different tissues is expected. All these results are represented in Fig. 4.

The parameters $MPS_{release}$ and $Cl_{int,MPS}$ were adjusted in our model considering *in vivo* tissue concentrations observed in rats [29, 30]. The value fitted to $MPS_{release}$ was 9×10^{-3} h^{-1}, 10 times higher than the value described by Silva et al., [21]. We fitted this value considering that Doxil® achieves maximum tissue concentrations around 24 and 48 hours, and after 72 hours starts to decrease. The

value fitted to $Cl_{int,MPS}$ was 2.16 x 10^{-8} mL/h/cell, 10 times lower than the value described by Silva et al., [21] since Doxil® is a stealth liposome, and the surface polymer chains reduce the interaction of the liposomes with the mononuclear phagocytic system.

Prediction of tissue distribution in rats and humans

The time to maximum concentration (t_{max}) in tissues for doxorubicin in both rat and human models was before 30 minutes of administration, while for Doxil® the t_{max} was after 24 hours of administration, as demonstrated in Fig. 5.

The organs that accumulate most NP are spleen, liver, and lungs, in both models. The predicted C_{max} concentration of doxorubicin in the heart is much higher compared to the administration of Doxil® in both models (Fig. 5), potentially indicating a concentration dependent mechanism related to cardiac toxicity [20].

Discussion

The accumulation of liposomes in the tumour tissue is influenced by the enhanced systemic half-life and the liposome extravasation through blood vessels. Although the factors contributing to enhanced liposomal drug delivery to tumours as compared with the free drug in humans are not fully characterised, an increasing number of studies have described these processes in preclinical models. The investigation of the liposomal distribution in tissues in humans, is complicated by the requirement of imaging analysis with radiolabelled liposomes or for invasive procedures. The m-PBPK model proposed in this work is an important tool to rationalise the mechanisms regulating the liposomal tissue distribution and support the bridging of preclinical data.

A well-established correlation between liposome extended half-life and tumour uptake has been previously described [31, 32]. A similar correlation was implemented in the developed modelling approach for healthy tissues, where liposomes extravasate into the tissue extracellular fluid through pores in the microvessels and are localised mainly in the perivascular area with minimal uptake by tissue cells. As demonstrated in the predictions of tissue accumulation with the administration of Doxil® in rats and humans the organs that are characterised by higher vascular permeability (spleen and liver) also accumulated more Doxil®. Long-circulating liposomes allow the repeated passage through the tissue's microvascular bed. The higher permeability of leaky tumour vasculature compared to healthy tissues determines an enhanced accumulation and localization of liposome with liposome extended half-life

The lungs are characterised by the microvascular bed with limited fenestration [17, 18], but the accumulation of Doxil® is comparable to other tissues with higher vascular permeability. The presence of tissue-associated macrophages could also contribute to liposomal uptake, and this is one of the reasons that tissues like lungs, spleen, and liver present a higher accumulation of Doxil® compared to other organs. Once localised in the tissue, liposomes release the drug which determines drug diffusion into the

tissue compartment. The time dependent kinetics of these processes are not well characterized and may vary between different tissues.

The simulated pharmacokinetics in both rats and humans is comparable to the available quantitative data, where the half-life of Doxil® is longer in humans (45 hours) than in rodents (≈ 20 hours) or other animal species like dogs (≈ 30 hours), for instance. The increased half-life is the primary factor defining a 300-fold difference in AUC compared to free doxorubicin [27]. Additionally, the parameters Cl and Vd were lower for Doxil® than for free doxorubicin. The k_{deg} assumed in the model predicted accurately the release of doxorubicin since practically all of the predicted circulating drug (> 98%), in both rats and human models, is liposome encapsulated. The same was observed by Gabizon et al., [25] indicating that the pharmacokinetics of liposomal doxorubicin is influenced by the liposome carrier and most of the drug is delivered to tissues in liposome-associated form. Thus, the peak concentrations of drug in free form after Doxil® administration did not exceed 0.10 mg/L for a dose of 50.0 mg/m^2 in humans and 0.01 mg/L for a dose of 1.0 mg/kg in rats and are substantially lower than after administration of the same dose of free doxorubicin (5.90 mg/L in humans and 0.33 mg/L in rats).

An important advantage of liposomal entrapment of doxorubicin is its reduced uptake in the heart compared with free doxorubicin. Since part of doxorubicin-induced cardiotoxicity appears to be related to a high peak concentration of free drug [33], the predicted lower free drug peak concentrations following Doxil administration can provide a rational explanation for the low observed cardiotoxicity.

Although the PK of Doxil in rats and human was successfully predicted, the model has some limitations. The *in vitro* parameters $MPS_{release}$ and $Cl_{int,MPS}$ used as input for the model were not specific to Doxil®, erythrocyte and protein binding was assumed to be minimal, and a more detailed experimental description of key ADME mechanisms could support a more relevant simulation of time dependent processes.

Conclusion

The integration of a quantitative description of NP ADME with pharmacokinetic-pharmacodynamic data can define a predictive framework to rationalize the design of materials to enhance drug delivery. This can also provide a guide for clinicians on the choice of optimal dose, and/or regimen for different tumour types when coupled to reduced side-effects.

Declarations

Ethics approval and consent to participate:

No ethical approval is required for this study.

Consent for publication:

All authors have agreed with publication of the manuscript.

Availability of data and materials:

Raw data and the model code are available from the corresponding author on request.

Competing interests:

The authors declare no competing interests.

Funding:

This work was partially supported by the European Union H2020 framework programme under the REFINE project (Grant agreement ID: 761104).

Authors' contributions:

All authors contributed to the overall concept of the model. All authors reviewed and contributed to the final manuscript.

Acknowledgements:

Not applicable.

References

1. Ariën A, Stoffels P. History: potential, challenges, and future development in nanopharmaceutical research and industry. In: Pharmaceutical Nanotechnology: Innovation and Production [Internet]. Weinheim, Germany: Wiley-VCH Verlag GmbH & Co. KGaA; 2016. p. 1–16.
2. Hutchinson CR, Colombo AL. Genetic engineering of doxorubicin production in Streptomyces peucetius: a review. J Ind MicrobiolBiotechnol. 1999 Jul 1; 23(1): 647–52.
3. Ashford M. Development and Commercialization of Nanocarrier-Based Drug Products. In: Pharmaceutical Nanotechnology: Innovation and Production [Internet]. Weinheim, Germany: Wiley-VCH Verlag GmbH & Co. KGaA; 2016. p. 697–734.
4. Maeda H, Wu J, Sawa T, Matsumura Y, Hori K. Tumor vascular permeability and the EPR effect in macromolecular therapeutics: a review. J Controlled Release. 2000 Mar; 65(1–2): 271–84.
5. Bozzuto G, Molinari A. Liposomes as nanomedical devices. Int J Nanomedicine. 2015 Feb; 975.
6. Bor G, Mat Azmi ID, Yaghmur A. Nanomedicines for cancer therapy: current status, challenges and future prospects. TherDeliv. 2019 Feb; 10(2): 113–32.
7. Barenholz Y (Chezy). Doxil® — The first FDA-approved nano-drug: Lessons learned. J Controlled Release. 2012 Jun; 160(2): 117–34.

8. Moss DM, Siccardi M. Optimizing nanomedicine pharmacokinetics using physiologically based pharmacokinetics modelling. Br J Pharmacol 2014; 171:1–17.
9. Dogra, P. et al. (2020). A mathematical model to predict nanomedicine pharmacokinetics and tumor delivery. Computational and structural biotechnology journal, 18, 518-531.
10. Peters, S. A. (2012). Physiologically-based pharmacokinetic (PBPK) modeling and simulations: principles, methods, and applications in the pharmaceutical industry. John Wiley & Sons.
11. Shah, D. K., & Betts, A. M. (2012). Towards a platform PBPK model to characterize the plasma and tissue disposition of monoclonal antibodies in preclinical species and human. Journal of pharmacokinetics and pharmacodynamics, 39(1), 67-86.
12. Gill, K. L., Gardner, I., Li, L., &Jamei, M. (2016). A bottom-up whole-body physiologically based pharmacokinetic model to mechanistically predict tissue distribution and the rate of subcutaneous absorption of therapeutic proteins. The AAPS journal, 18(1), 156-170.
13. Centers for Disease Control and Prevention. Available from: https://www.cdc.gov/growthcharts/clinical_charts.htm.
14. Bosgra, S., et al., An improved model to predict physiologically based model parameters and their inter-individual variability from anthropometry. Crit Rev Toxicol, 2012. 42(9): p. 751-67.
15. Physiological Parameter Values for PBPK models. 1994; Available from: 9100K030.PDF (epa.gov).
16. Yuan, D., He, H., Wu, Y., Fan, J., & Cao, Y. (2019). Physiologically based pharmacokinetic modeling of nanoparticles. Journal of pharmaceutical sciences, 108(1), 58-72.
17. Sarin, H. (2010). Physiologic upper limits of pore size of different blood capillary types and another perspective on the dual pore theory of microvascular permeability. Journal of angiogenesis research, 2(1), 1-19.
18. Bachler, G., von Goetz, N., &Hungerbühler, K. (2013). A physiologically based pharmacokinetic model for ionic silver and silver nanoparticles. International journal of nanomedicine, 8, 3365.
19. Poulin, P. and F.P. Theil, Prediction of pharmacokinetics prior to in vivo studies. 1. Mechanism-based prediction of volume of distribution. J Pharm Sci, 2002. 91(1): p. 129-56.
20. Working, P. K., Newman, M. S., Huang, S. K., Mayhew, E., Vaage, J., &Lasic, D. D. (1994). Pharmacokinetics, biodistribution and therapeutic efficacy of doxorubicin encapsulated in Stealth® liposomes (Doxil®). Journal of Liposome Research, 4(1), 667-687.
21. Silva, A. H., Lima Jr, E., Mansilla, M. V., Zysler, R. D., Pisciotti, M. L. M., Locatelli, C., ... & Siccardi, M. (2017). A physiologically based pharmacokinetic model to predict the superparamagnetic iron oxide nanoparticles (SPIONs) accumulation in vivo. European Journal of Nanomedicine, 9(2), 79-90.
22. Xiong, X. B., Huang, Y., Lu, W. L., Zhang, X., Zhang, H., Nagai, T., & Zhang, Q. (2005). Enhanced intracellular delivery and improved antitumor efficacy of doxorubicin by sterically stabilized liposomes modified with a synthetic RGD mimetic. Journal of controlled release, 107(2), 262-275.
23. Doxorubicin. Available at: https://go.drugbank.com/drugs/DB00997.

24. Terasaki, T., Igax, T., Sugiyama, Y., & Hanano, M. (1984). Pharmacokinetic study on the mechanism of tissue distribution of doxorubicin: interorgan and interspecies variation of tissue-to-plasma partition coefficients in rats, rabbits, and guinea pigs. Journal of pharmaceutical sciences, 73(10), 1359-1363.
25. Gabizon, A., Catane, R., Uziely, B., Kaufman, B., Safra, T., Cohen, R., ... &Barenholz, Y. (1994). Prolonged circulation time and enhanced accumulation in malignant exudates of doxorubicin encapsulated in polyethylene-glycol coated liposomes. Cancer research, 54(4), 987-992.
26. Rahman, A., Carmichael, D., Harris, M., &Roh, J. K. (1986). Comparative pharmacokinetics of free doxorubicin and doxorubicin entrapped in cardiolipin liposomes. Cancer research, 46(5), 2295-2299.
27. Gabizon, A., Shmeeda, H., & Barenholz, Y. (2003). Pharmacokinetics of pegylated liposomal doxorubicin. Clinical pharmacokinetics, 42(5), 419-436.
28. Gabizon, A., & Martin, F. (1997). Polyethylene glycol-coated (pegylated) liposomal doxorubicin. Drugs, 54(4), 15-21.
29. Soundararajan, A., Bao, A., Phillips, W. T., Perez III, R., & Goins, B. A. (2009). [186Re] Liposomal doxorubicin (Doxil): in vitro stability, pharmacokinetics, imaging and biodistribution in a head and neck squamous cell carcinoma xenograft model. Nuclear medicine and biology, 36(5), 515-524.
30. Burade, V., Bhowmick, S., Maiti, K., Zalawadia, R., Jain, D., &Rajamannar, T. (2017). Comparative plasma and tissue distribution of Sun Pharma's generic doxorubicin HCl liposome injection versus Caelyx®(doxorubicin HCl liposome injection) in syngeneic fibrosarcoma-bearing BALB/c mice and Sprague–Dawley rats. Cancer chemotherapy and pharmacology, 79(5), 899-913.
31. Huang SK, Lee KD, Hong K, et al. Microscopic localization of sterically stabilized liposomes in colon carcinoma-bearing mice. Cancer Res 1992; 52: 5135-43.
32. Yuan F, Leunig M, Huang SK, et al. Microvascular permeability and interstitial penetration of sterically stabilized (Stealth) liposomes in a human tumor xenograft. Cancer Res 1994; 54: 3352-6.
33. Legha SS, Benjamin RS, Mackay B, et al. Reduction of doxorubicin cardiotoxicity by prolonged continuous intravenous infusion. Ann Intern Med 1982; 96: 133-9.

Figures

Figure 1

Schematic diagram of the whole-body m-PBPK models developed for Doxil® and doxorubicin. MPS representsmacrophage cells.Yellow arrows represent lymph flow ($Q_{L,organ}$).Red and blue arrows represent arterial and venous blood flow. In the NP representation venous blood flow correspond to the Q_{organ}-$Q_{L,organ.}$ Black and green dashed arrows correspond to the release of the drug into compartments and macrophage (k_{deg}, $MPS_{release}$), respectively.Systemic clearance of doxorubicin is represented as the sum of hepatic and renal clearance.

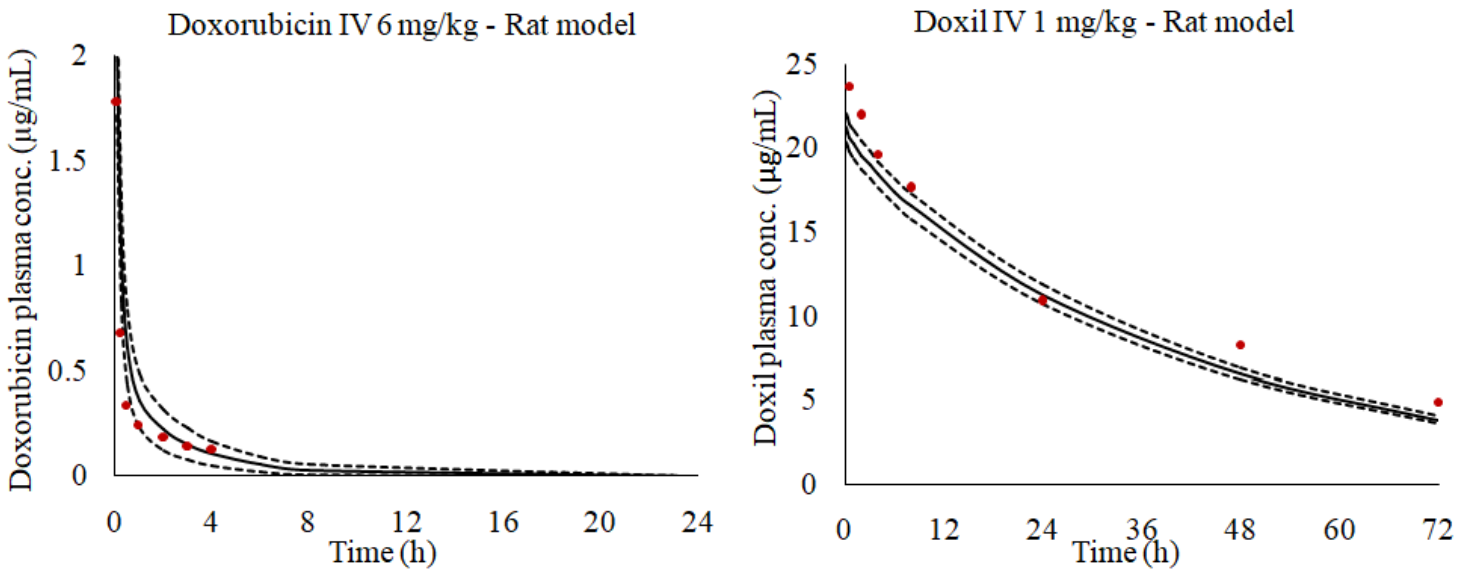

Figure 2

Qualification of the rat model with administration of doxorubicin IV 6 mg/kg and Doxil IV 1 mg/kg. Black line represents mean predicted plasma concentration over time, dashed black lines represent the predicted mean ± SD, and red dots represents the observed data extracted from literature [26, 28].

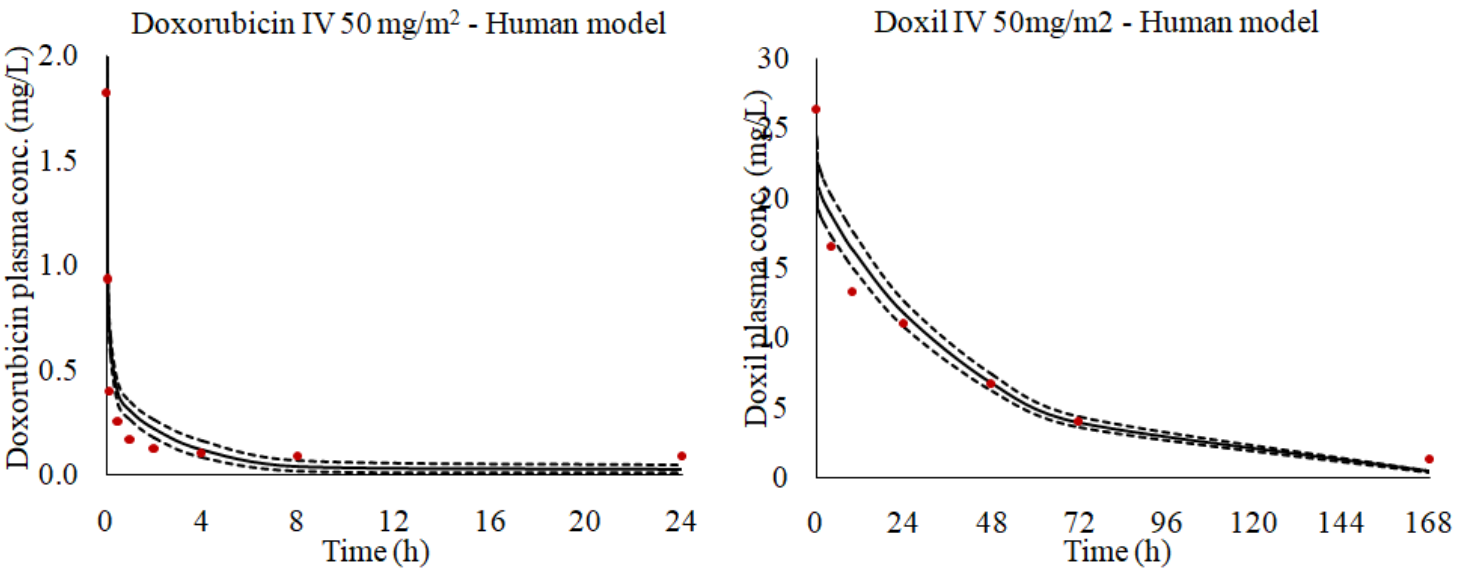

Figure 3

Qualification of the human model with administration of doxorubicin and Doxil IV 50 mg/m^2. Black line represents mean predicted plasma concentration over time, dashed black lines representthe predicted mean ± SD, and red circles the observed data [27].

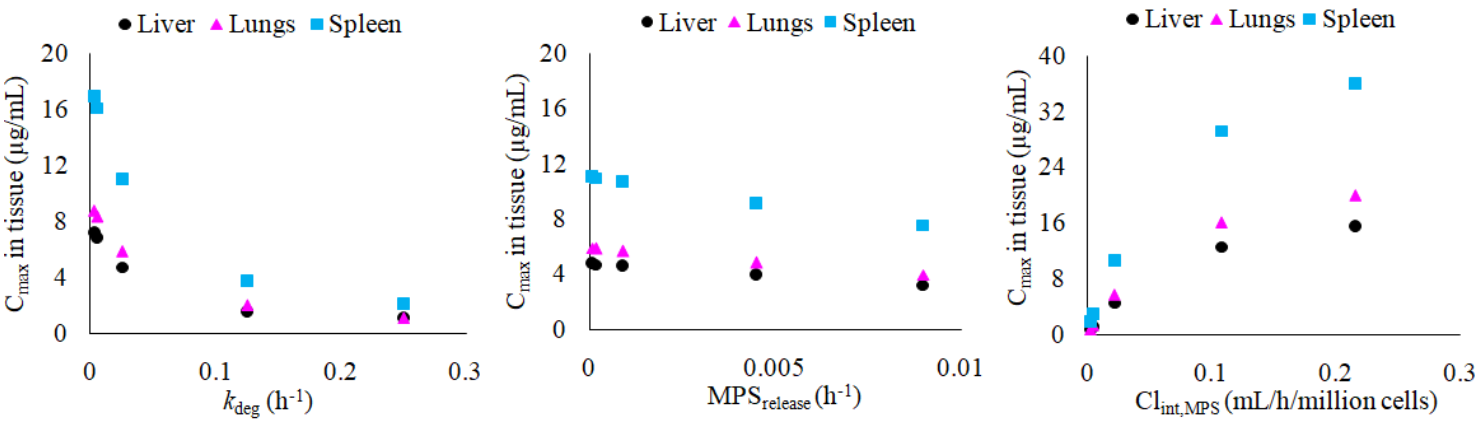

Figure 4

Sensitivity analysis of the rat model considering changes of ±10 fold or ±5 fold compared to the initial values to the parameters: k_{deg}(0.025 h^{-1}), $MPS_{release}$(9 x $10^{-4}h^{-1}$), $Cl_{int,MPS}$(2.16 x 10^{-2}mL/h/million cells). Doxil® maximum concentration was calculated at 24 h in the liver, spleen, and lungs.

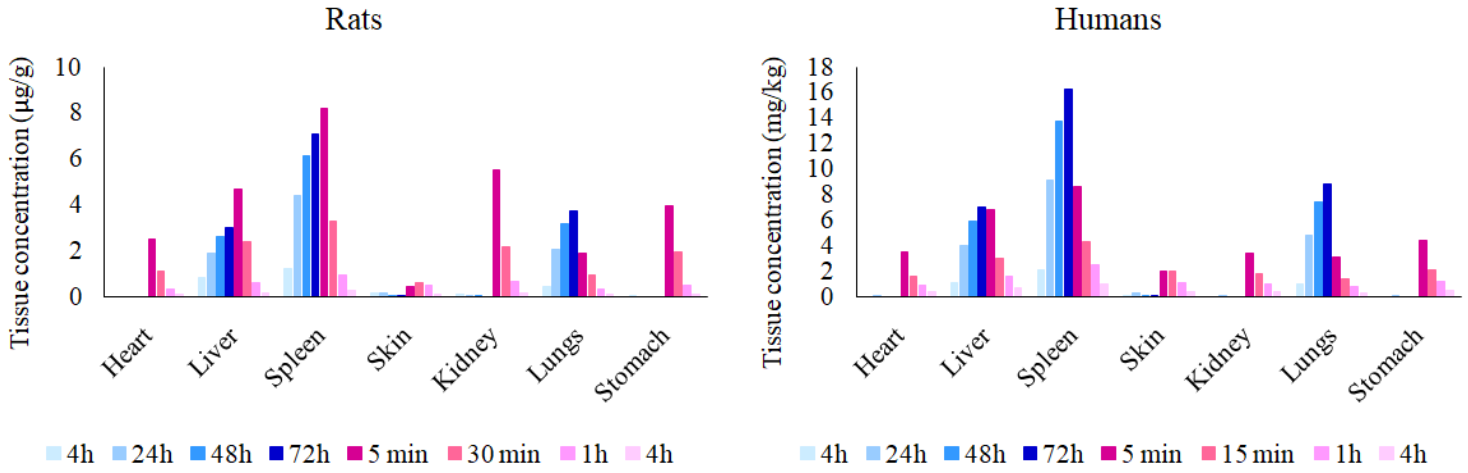

Figure 5

Predictions of tissue accumulation with administration of 1 mg/kg of IVdoxorubicin (pink bars) and Doxil® (blue bars) in rats (left hand side plot). Whereas the right hand-side plot report on the predition of tissue accumulation withadministration of 50 mg/m^2 of IV doxorubicin (pink bars) and Doxil® (blue bars) in humans.

Supplementary Files

This is a list of supplementary files associated with this preprint. Click to download.

- Graphicalabstract.png